

A&A manuscript no.  
(will be inserted by hand later)

Your thesaurus codes are:  
(02.01.2; 08.09.2; 08.14.1; 13.25.5)

ASTRONOMY  
AND  
ASTROPHYSICS

# Broad-band BeppoSAX observation of the low-mass X-ray binary X 1822-371

A.N. Parmar<sup>1</sup>, T. Oosterbroek<sup>1</sup>, S. Del Sordo<sup>2</sup>, A. Segreto<sup>2</sup>, A. Santangelo<sup>2</sup>, D. Dal Fiume<sup>3</sup>, and M. Orlandini<sup>3</sup>

<sup>1</sup> Astrophysics Division, Space Science Department of ESA, ESTEC, P.O. Box 299, 2200 AG Noordwijk, The Netherlands

<sup>2</sup> IFCAI, CNR, via La Malfa 153, I-90146 Palermo, Italy

<sup>3</sup> Istituto TESRE, CNR, via Gobetti 101, I-40129 Bologna, Italy

Received: 1999 November 10; Accepted: 2000 January 13

**Abstract.** Results of a 1997 September 9–10 BeppoSAX observation of the 5.57 hr low-mass X-ray binary (LMXRB) X 1822-371 are presented. The 0.3–40 keV spectrum is unusually complex and cannot be fit by any of the standard models applied to other LMXRB. At least two components are required. One component has a shape consistent with that expected from the Comptonization of an input soft (Wien) spectrum while the other, contributing  $\gtrsim 40\%$  of the 1–10 keV flux, is consistent with being a blackbody. In addition, there is a “dip” in the spectrum which can be modeled by a  $1.33 \pm_{0.11}^{0.05}$  keV absorption edge with an optical depth,  $\tau$ , of  $0.28 \pm 0.06$ . If the same model is fit to ASCA Solid-State Imaging Spectrometer spectra obtained in 1993 and 1996, then reasonable fits are also obtained, with a similar absorption feature required. The nature of this feature is highly uncertain; its energy corresponds to the K-edges of highly ionized Ne X and neutral Mg, or to an L-edge of moderately ionized Fe. Surprisingly, no strong ( $\tau > 0.05$ ) Fe-K or ( $\tau > 0.18$ ) O-K edges are visible. The folded lightcurve of X 1822-371 is similar to previous observations, except that no strong softening is seen near the eclipse. An updated orbital ephemeris is provided.

**Key words:** accretion, accretion disks – Stars: individual: X 1822-371 – Stars: neutron – X-rays: stars

## 1. Introduction

The 5.57 hr low-mass X-ray binary (LMXRB) X 1822-371 is viewed almost edge on with the central X-ray source hidden by material in the orbital plane. The X-ray lightcurve shows a partial eclipse and a smooth broad modulation with a minimum just prior to the eclipse (White et al. 1981). The partial nature of the eclipse indicates that the X-ray emitting region is extended, and that the observed

X-rays are scattered in an accretion disk corona, or ADC (White & Holt 1982). The optical lightcurve has a similar morphology except that the eclipse is broader. White & Holt (1982) showed that the broad X-ray modulation can be modeled as obscuration of the ADC by the rim of the accretion disk whose thickness is greatest near phase,  $\Phi$ , 0.8 (where  $\Phi = 0.0$  is mid-eclipse), and least near  $\Phi = 0.2$ . Modeling of multi-wavelength lightcurves reveals that the effective diameter of the ADC is  $3 \times 10^{10}$  cm, about half that of the optically emitting disk, and that structure in the disk can reach a height of  $1.5 \times 10^{10}$  cm (White & Holt 1982; Mason & Córdova 1982; Hellier & Mason 1989; Puchnarewicz et al. 1995). No pulsations or bursts have been detected from X 1822-371 (e.g., Hellier et al. 1992). The probable distance to X 1822-371 is 2–3 kpc and the isotropic luminosity  $10^{36}(d_2)^2$  erg s<sup>-1</sup> (Mason & Córdova 1982), where  $d_2$  is distance in units of 2 kpc. The mean X 1822-371  $L_x/L_{\text{opt}}$  ratio of 20 compared to the average for LMXRB of 500 (van Paradijs & McClintock 1995) implies a unobscured luminosity of  $2 \times 10^{37}(d_2)^2$  erg s<sup>-1</sup>, similar to that observed from the brighter X-ray burst sources.

The X-ray spectrum of X 1822-371 is complex with different results being obtained from different measurements. The 2–40 keV HEAO-1 A2 spectrum can be fit by a power-law with a photon index,  $\alpha$ , of 1.3, a high-energy cutoff at 18 keV, and a broad Fe-K line with a full-width half maximum (FWHM) of 4 keV. Below 2 keV there is evidence for an excess in the *Einstein* Solid State Spectrometer spectrum which White et al. (1981) can model as a 0.25 keV thermal bremsstrahlung, a 0.16 keV blackbody or a 350 eV equivalent width (EW) emission feature at 0.8 keV. The combined 0.04–20 keV EXOSAT Channel Multiplier Array and Medium Energy Detector Array spectrum is fit by a power-law with  $\alpha = 0.8$  together with a blackbody with  $kT = 1.8$  keV and a  $\sim 1$  keV FWHM Fe-K line (Hellier & Mason 1989). Subsequently, Hellier et al. (1992) obtained a *Ginga* 1.5–30 keV spectrum, but were unable to find a satisfactory fit, although the model used for the EXOSAT spectrum gives the best result.

Send offprint requests to: A.N. Parmar (aparmar@astro.estec.esa.nl)

White et al. (1997) report on an ASCA observation of X 1822-371. The best-fit Solid-State Imaging Spectrometer (SIS) and Gas Imaging Spectrometer (GIS) 0.5–10 keV spectrum is also complex and cannot be easily fit by any of the standard models. White et al. (1997) characterize the spectrum using a power-law continuum with  $\alpha \sim 0.52$ . Structured residuals remain with a pronounced dip at  $\sim 1.5$  keV and a strong decrease  $\gtrsim 7$  keV. There are no emission features present other than two weak features at 6.4 keV and 7.1 keV, consistent with Fe  $K\alpha$  and  $K\beta$  lines. The EW of the  $K\alpha$  line is  $\sim 40$  eV. However, as White et al. (1997) note, the observed  $K\beta/K\alpha$  ratio of  $\sim 40\%$  does not match the theoretical value of 13%. White et al. (1997) attempt to model the reduction in observed flux  $\gtrsim 7$  keV by an Fe-K absorption edge, but find that edges from a range of ionization states are necessary to explain the observed shape.

As White et al. (1997) point out, accurately measuring the continuum  $\gtrsim 10$  keV is vital in order to constrain the Fe-K absorption feature seen in the ASCA spectrum. Indeed, these authors used non-simultaneous EXOSAT and *Ginga* data to try to do this, but were unsuccessful. We report here on a BeppoSAX observation of X 1822-371 where the 0.3–40 keV spectrum was observed simultaneously with good sensitivity. We compare the results of the BeppoSAX spectral fits with those obtained by White et al. (1997) and those obtained from a subsequent ASCA observation.

## 2. Observations

Results from the Low-Energy Concentrator Spectrometer (LECS; 0.1–10 keV; Parmar et al. 1997), the Medium-Energy Concentrator Spectrometer (MECS; 1.8–10 keV; Boella et al. 1997), the High Pressure Gas Scintillation Proportional Counter (HPGSPC; 5–120 keV; Manzo et al. 1997) and the Phoswich Detection System (PDS; 15–300 keV; Frontera et al. 1997) on-board BeppoSAX are presented. All these instruments are coaligned and collectively referred to as the Narrow Field Instruments, or NFI. The MECS consists of two grazing incidence telescopes with imaging gas scintillation proportional counters in their focal planes. The LECS uses an identical concentrator system as the MECS, but utilizes an ultrathin entrance window and a driftless configuration to extend the low-energy response to 0.1 keV. The non-imaging HPGSPC consists of a single unit with a collimator that was alternatively rocked on- and 180° off-source every 96 s during the observation. The non-imaging PDS consists of four independent units arranged in pairs each having a separate collimator. Each collimator was alternatively rocked on- and 210° off-source every 96 s during the observation.

The region of sky containing X 1822-371 was observed by BeppoSAX on 1997 September 09 12:24 UT to September 10 11:47 UT. Good data were selected in the standard

way using the SAXDAS 2.0.0 data analysis package. LECS and MECS data were extracted centered on the (on-axis) position of X 1822-371 using radii of 8' and 4', respectively. The exposures in the LECS, MECS, HPGSPC, and PDS instruments are 14.8 ks, 37.0 ks, 19.5 ks, and 18.7 ks, respectively. Background subtraction for the imaging instruments was performed using standard files, but is not critical for such a bright source. Background subtraction for the HPGSPC was carried out using data obtained when the instrument was looking at the dark Earth and for the PDS using data obtained during intervals when the collimator was offset from the source.

The BeppoSAX data is compared with results from the Solid State Imaging Spectrometers SIS0 and SIS1 (0.6–10 keV), on-board ASCA (Tanaka et al. 1994). The energy resolution of the SIS is a factor of a few better, except at the lowest energies, than that of the LECS and MECS. ASCA observed X 1822-371 twice. The first observation took place between 1993 October 07 03:33 and 23:55 UTC and the second between 1996 September 26 05:44 and September 27 08:05 UTC. The SIS exposures for each observation are 36.6 ks and 26.0 ks both using 1-CCD BRIGHT mode. All data were screened and processed using the standard Rev2 pipeline. The source count rates of  $\lesssim 6.5 \text{ s}^{-1} \text{ SIS}^{-1}$  means that pulse pile-up is unlikely to be significant.

## 3. Analysis and results

### 3.1. BeppoSAX lightcurve

Background subtracted lightcurves in the energy ranges 1.8–4 keV (MECS), 4–10 keV (MECS), 10–16 keV (HPGSPC) and 16–32 keV (PDS) were extracted and folded using the linear ephemeris of Hellier & Smale (1994). Fig. 1 shows these lightcurves together with two hardness ratios (4–10 keV counts divided by 1.8–4 keV counts and 16–32 keV counts divided by 10–16 keV counts). The lightcurves are similar to those reported previously, showing gradual reductions in flux which reach minima around  $\Phi \sim 0.8$ , before the partial eclipse and rapid increases following egress. Just prior to the partial eclipse each lightcurve shows a narrow increase in flux. The depth of the partial eclipse increases with increasing energy. There are no strong variations in hardness ratio. However, the 4–8 keV/1.8–4 keV hardness ratio (HR1) shows a broad variation with a maximum around  $\Phi \sim 0.4$ , as well as a narrow increase just prior to eclipse. Instead, the 16–32 keV/8–16 keV hardness ratio (HR2) does not vary appreciably with phase, except between  $\Phi = 0.7$ –1.1 where a harder interval, punctuated by the eclipse, is present. HR1 is similar in shape to the 6–30 keV/1–6 keV hardness ratio obtained from *Ginga* observations (see Fig. 1 of Hellier et al. 1992), except that no strong softening is visible in the BeppoSAX data during the eclipse. This is in contrast to previous results, where the eclipse depths measured by EXOSAT and *Ginga* both

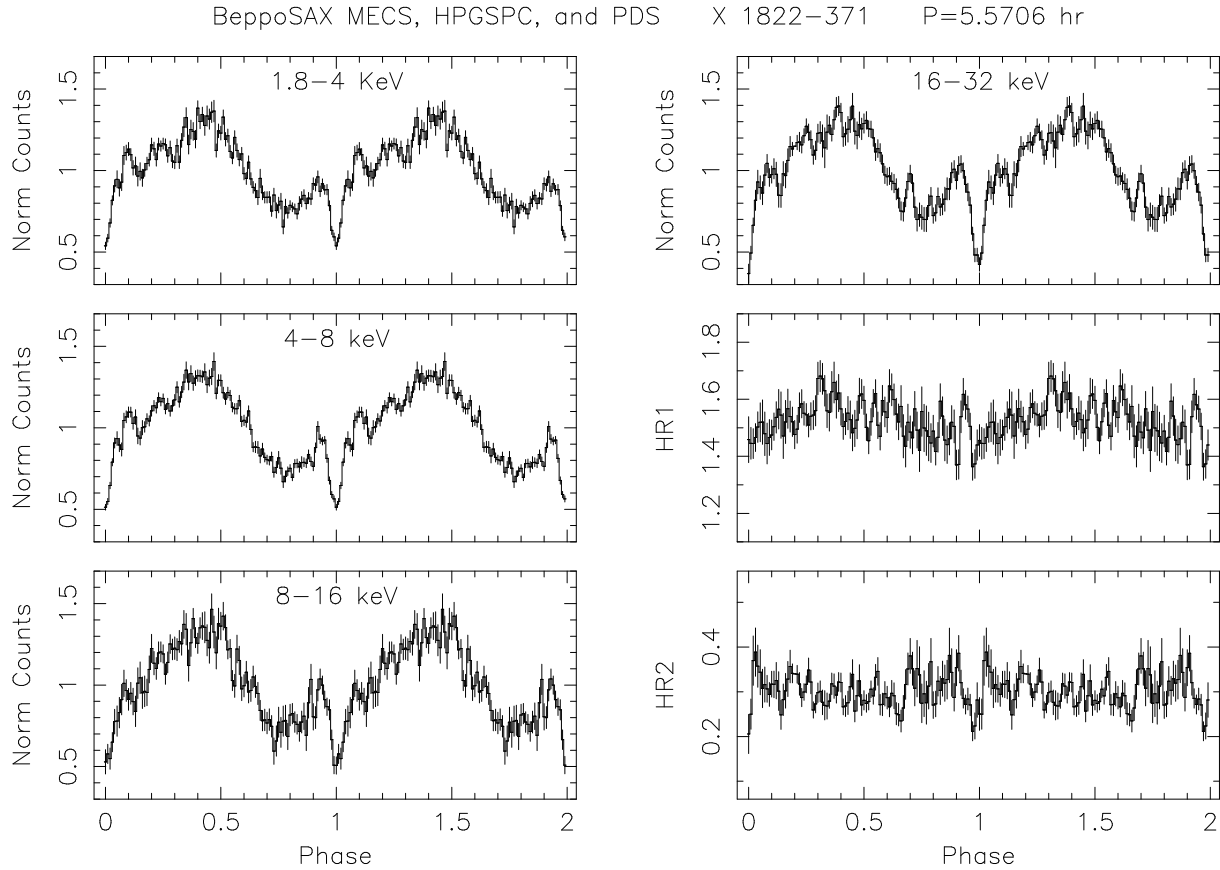


**Fig. 1.** The X1822-371 folded lightcurves and hardness ratios. The energy ranges are indicated. The upper two left panels have 100 phase bins, the others 50. HR1 and HR2 are the 4–8 keV/1.8–4 keV and 16–32 keV/10–16 keV hardness ratios, respectively. The ordinate extrema of each lightcurve are normalized to the mean count rate for ease of comparison

showed a similar strong dependence on energy (Hellier et al. 1992). The lack of any large change in the BeppoSAX hardness ratios justifies the use of the entire data set in the spectral analysis in Sect. 3.3.

### 3.2. Eclipse timing

Eclipse arrival times using recent BeppoSAX MECS, ASCA and RXTE Proportional Counter Array data have been determined. Since there are substantial gaps in the data and the count rates low, the BeppoSAX and ASCA lightcurves were first folded on the 5.5706 hr period of Hellier & Smale (1994). A model consisting of a Gaussian and a constant was then fit to the eclipse phases ( $\Phi = 0.95$ – $1.05$ ) of the folded lightcurves. The arrival time of the eclipse was then assigned to the eclipse which occurred closest to mid-time of the observation. For the MECS the uncertainty on the arrival time was obtained directly from the fit. Data from the 4 ASCA instruments were analyzed independently and the uncertainties in the arrival times were derived from the spreads in the obtained values, while the arrival times were defined as the averages from the 4 instruments. The RXTE observation was made between

1996 September 26 16:03 and September 27 07:19 UTC. Since only one eclipse was observed, the Gaussian and a constant model was fit directly to the eclipse interval in the lightcurve. The uncertainty in the RXTE arrival time was estimated by comparing results obtained using (1) a range of eclipse phases around those given above using the Gaussian and constant model and (2) including a linear term in the above model and fitting over the same range of phases. The spread in values obtained using these two methods was larger than the uncertainties obtained from the individual fits, and so was adopted as an estimate of the overall uncertainty. The fit results, which extend the measurements in Hellier & Smale (1994) by some 5 yrs, or 8000 cycles, are summarized in Table 1.

The newly determined arrival times together with the measurements tabulated in Hellier & Smale (1994) were fit to obtain an updated ephemeris. Both linear ( $\chi^2 = 98.5$  for 17 dof) and quadratic ephemerides ( $\chi^2 = 21.4$  for 16 dof) were used. The difference in reduced  $\chi^2$  indicates that the quadratic term in the ephemeris is established with 99.9999% confidence. Fig. 2 shows the residuals with respect to both ephemerides. The updated quadratic ephemeris is given by:

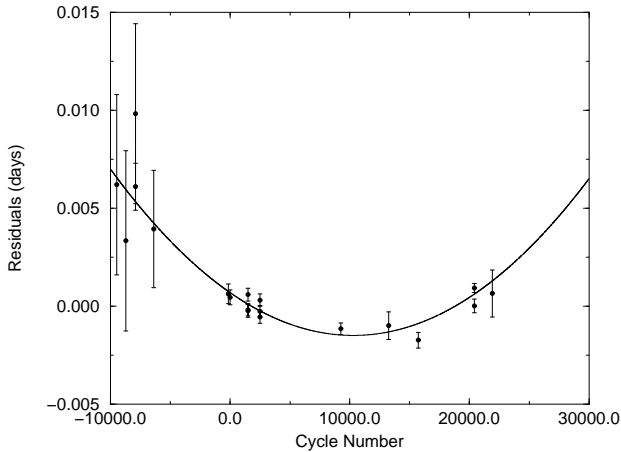


**Fig. 2.** The X 1822-371 partial eclipse timing residuals with respect to the best-fit linear ephemeris (small filled circles). The quadratic ephemeris (solid line) is also indicated

**Table 1.** New X-ray eclipse times for X 1822-371. A compilation of previous measurements can be found in Hellier & Smale (1994). Uncertainties are given at 68% confidence

JD <sub>⊙</sub>	Uncertainty	Cycle	Satellite
2,449,268.00984	0.00040	15737	ASCA
2,450,353.35425	0.00035	20412	ASCA
2,450,353.58728	0.00023	20414	RXTE
2,450,701.51870	0.00120	21912	BeppoSAX

$$T_{\text{ecl}} = 2445615.30964(15) + 0.232108785(50)N \\ + 2.06(23) \times 10^{-11} N^2.$$

### 3.3. BeppoSAX spectrum

The overall spectrum of X 1822-371 was first investigated by simultaneously fitting data from all the BeppoSAX NFI. All spectra were rebinned using standard procedures. Data were selected in the energy ranges 0.3–4.0 keV (LECS), 2.0–10 keV (MECS), 7.0–30 keV (HPGSPC), and 15–40 keV (PDS) where the instrument responses are well determined and sufficient counts obtained. This gives background-subtracted count rates of 1.0, 4.2, 8.8 and 4.0 s<sup>-1</sup> for the LECS, MECS, HPGSPC, and PDS, respectively. The photo-electric absorption cross sections of Morisson & McCammon (1983) and the abundances of Anders & Grevesse (1989) are used throughout. Factors were included in the spectral fitting to allow for normalization uncertainties between the instruments. These factors

**Table 2.** Best-fit to the BeppoSAX NFI spectrum. The model consists of absorbed blackbody and COMPTT continuum, a Gaussian emission line, and an absorption edge

Parameter	
N <sub>H</sub> (atom cm <sup>-2</sup> )	$(1.2 \pm_{1.2}^{0.8}) \times 10^{20}$
Blackbody kT (keV)	$1.88 \pm 0.02$
kT <sub>e</sub> (keV)	$4.52 \pm 0.02$
τ <sub>p</sub>	$26.1 \pm 0.5$
kT <sub>w</sub> (keV)	$0.15 \pm 0.02$
Line energy (keV)	$6.57 \pm_{0.07}^{0.04}$
Line FWHM (keV)	$0.69 \pm 0.19$
Line EW (keV)	$0.150 \pm 0.025$
Edge energy (keV)	$1.33 \pm_{0.11}^{0.05}$
Edge τ	$0.28 \pm 0.06$
χ <sup>2</sup> /dof	122.1/125

were constrained to be within their usual ranges during the fitting. All spectral uncertainties and upper-limits are given at 90% confidence.

Initially, a standard LMXRB spectral model consisting of a cutoff power-law ( $E^{-\alpha} \exp(-E_c/kT)$ ) appropriate to low-luminosity sources was fit to the BeppoSAX spectrum. Since the central X-ray source in X 1822-371 is hidden from direct view the overall luminosity of X 1822-371 is highly uncertain, and an additional blackbody component, frequently observed in more luminous LMXRB (e.g., White et al. 1988) was also included. The cutoff power-law model gives an unacceptable fit with a χ<sup>2</sup> of 670 for 133 dof. Adding a 1.5 keV blackbody reduces the χ<sup>2</sup> to 596 for 131 dof. Inspection of the residuals indicated the presence of an Fe-K line. Adding a broad line at ~6.5 keV further reduces the χ<sup>2</sup> to 408 for 128 dof. The remaining residuals are indicative of an intense low-energy excess. We attempted to model this feature using a Gaussian emission line, thermal bremsstrahlung, blackbody and power-law components. Only the fit including a Gaussian feature was acceptable with a χ<sup>2</sup> of 144.5 for 125 dof. Thus, this model consists of a cutoff power-law with α = -0.78 ± 0.02 and E<sub>c</sub> = 5.69 ± 0.06 keV and a 1.27 ± 0.03 keV blackbody continuum together with two Gaussian emission features. The nature of the low-energy feature is highly uncertain. Its energy can only be constrained to be <0.50 keV, it is extremely broad (FWHM = 1.5 keV), and its EW is implausibly high (~7 keV). We therefore reject this model as being physically unreasonable.

The HEAO-1 X 1822-371 spectrum of White et al. (1981) is well fit above 2 keV using a power-law model with a high-energy break ( $\exp((E_{\text{cut}} - E)/E_{\text{fold}})$  for E > E<sub>cut</sub>) at 17 keV. Fitting this model to the BeppoSAX NFI spectrum does not produce an acceptable fit with a χ<sup>2</sup> of 1960 for 132 dof. If a blackbody is included, then the situation improves with a χ<sup>2</sup> of 342 for 130 dof. Including a broad Fe line decreases the χ<sup>2</sup> to 198.9 for 127 dof. The ma-

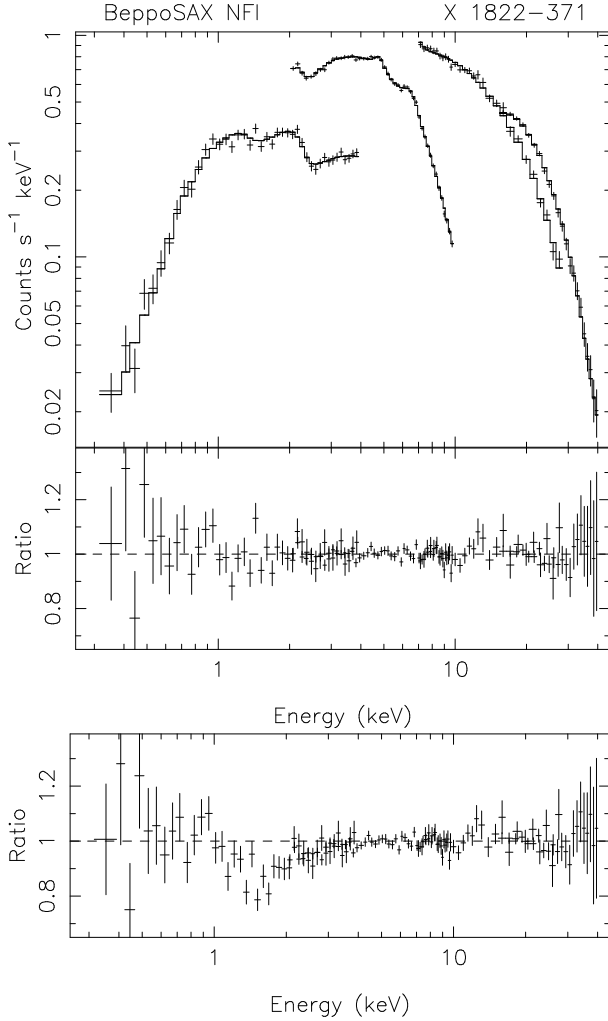


**Fig. 3.** The X 1822-371 count spectrum and residuals when a COMPTT and blackbody continuum with an edge and an Fe line are fit (Table 2). The middle panel shows the ratio of the data divided the model and the lower panel shows the same when the edge is excluded

major contribution to  $\chi^2$  comes from the region near 1 keV where the model overestimates the observed spectrum. We attempted to model feature this using partial covering (the PCFABS model in XSPEC, an ionized absorber the ABSORI model in XSPEC), and an absorption edge. Only the edge was successful with an energy of  $1.30 \pm 0.07$  keV and an optical depth,  $\tau$ , of  $0.35 \pm 0.09$  for a  $\chi^2$  of 139.4 for 125 dof. The best-fit value of  $E_{\text{cut}}$  of  $17.1 \pm 0.7$  keV is in good agreement with that obtained from HEAO-1 of  $17.4 \pm 0.5$  keV (White et al. 1981). There is no evidence for the presence of low-energy thermal components, Fe-L emission near 1 keV as proposed by White et al. (1981), or a reflection component (the PEXRAV model in XSPEC).

Finally, we investigated whether Comptonization models such as the XSPEC model COMPTT (Titarchuk 1994; Hua & Titarchuk 1995; Titarchuk & Lyubarskij 1995), which self-consistently calculate the spectrum produced

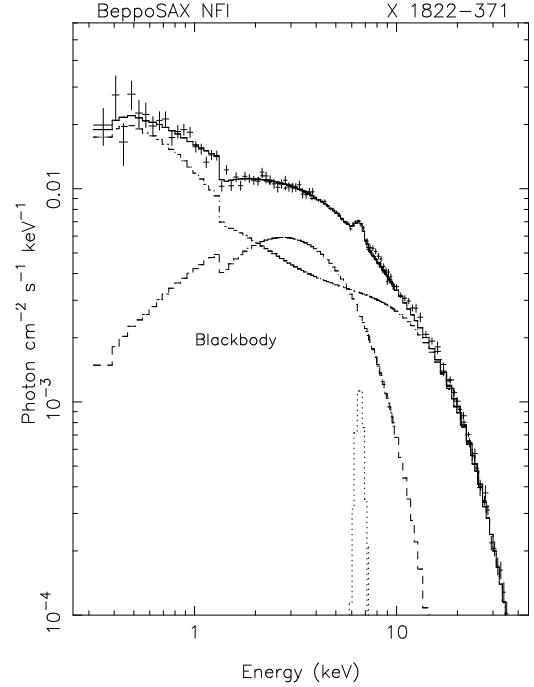


**Fig. 4.** The overall X 1822-371 NFI photon spectrum derived using the COMPTT and blackbody continuum with an edge and an Fe line. The individual contributions are indicated

by the Comptonization of soft photons in a hot plasma, could be applicable to X 1822-371. This model contains as free parameters the temperature of the Comptonizing electrons  $kT_e$ , the plasma optical depth with respect to electron scattering  $\tau_p$  and the input temperature of the soft photon (Wien) distribution  $kT_w$ . A spherical geometry was assumed for the Comptonizing region. This replaced the power-law and high-energy cutoff in the previous model and the fit repeated. A good fit is obtained with a  $\chi^2$  of 122.1 for 125 dof. The 1–10 keV flux is  $5.0 \times 10^{-10}$  erg cm $^{-2}$  s $^{-1}$  and the blackbody contributes 43% of the total flux in this energy range. The best-fit parameters are given in Table 2. If a disk geometry is assumed for the Comptonizing region, the best-fit parameters are essentially unchanged except for  $\tau_p$  which reduces to  $13.3 \pm 0.3$ . Fig. 3 shows the count spectra and the data/model ratios with, and without, the edge. The depth of the feature ( $\sim 20\%$ ) is significantly greater than the uncertainty in LECS calibration at the corresponding energies ( $\lesssim 5\%$ ). Fig. 4 shows the incident photon spectrum and illustrates how fitting a power-law in the energy range 1.0–10 keV would produce a “dip” at  $\sim 1.5$  keV as observed by White et al. (1997). The 90% confidence upper limits to the optical depths of any O-K and Fe-K edges at 0.54 keV and 7.1 keV are 0.18 and 0.05, respectively.

### 3.4. ASCA spectrum

We next examined whether the BeppoSAX best-fit model presented above is consistent with results from ASCA. For the 1993 ASCA observation these are presented in White et al. (1997). A simple power-law was first fit to the ASCA SIS spectra confirming that the overall shape of the spectrum is as reported in White et al. (1997) when using the latest processing. Next, the best-fit BeppoSAX model was fit to the SIS spectra. For the fit to the 1993 spectra an additional line feature at  $\sim 7$  keV was included. The results are presented in Table 3 and show that the best-fit BeppoSAX model also provides a reasonable fit to the ASCA SIS spectra. During the 1993 and 1996 observations, the 1–10 keV fluxes were  $5.8 \times 10^{-10}$  erg cm $^{-2}$  s $^{-1}$  and  $5.3 \times 10^{-10}$  erg cm $^{-2}$  s $^{-1}$ , and the blackbody contributed 48% and 47% of the flux in this energy range, respectively.

Comparing the best-fit parameters with those obtained with BeppoSAX reveals the following: (1) The overall spectral shape is similar in all three observations and may be modeled using COMPTT and blackbody continuum components. (2) There is a substantial (EW  $\sim 100$ –300 eV) Fe-K feature present which may be modeled as a broad feature at  $\sim 6.5$  keV, or as the sum of two narrower features at  $\sim 6.4$  keV and  $\sim 7.0$  keV. (3) Using the relation between optical and X-ray extinctions of Predehl & Schmitt (1995), all three best-fit absorptions are inconsistent with the value derived from the color excess of 0.13 in Mason et al. (1982) of  $8 \times 10^{20}$  atom cm $^{-2}$ . (4) All three spectra reveal clear evidence for a “dip” at  $\sim 1.3$  keV, which may be modeled by an absorption edge. The energies of this feature ( $1.33 \pm_{0.11}^{0.05}$  keV,  $1.37 \pm 0.03$  keV, and  $1.28 \pm 0.03$  keV) are in reasonable agreement, while there are clear variations in its optical depth ( $\tau = 0.28 \pm 0.06$ ,  $0.093 \pm 0.012$ , and  $0.15 \pm 0.02$ ).

## 4. Discussion

We present results of a 1997 September BeppoSAX observation of X 1822-371 and compare these with earlier ASCA observations when the source had a similar 1.0–10 keV intensity. The spectrum is unusually complex and cannot be fit by any of the usual models applied to LMXRB such as a cutoff power-law and blackbody unless an unusually strong low-energy emission feature is included. A good fit is obtained to the 0.3–40 keV BeppoSAX spectrum with the combination of a Comptonization component and a blackbody together with an Fe-K emission line and an absorption edge. The same model provides reasonable fits to ASCA SIS spectra with a similar absorption feature being required.

There are at least three highly unusual features of the X 1822-371 spectrum. The first, also pointed out by White et al. (1997), is that the continuum is much harder than is typical of similar luminosity LMXRBs, where  $\alpha$  is usually

**Table 3.** The best-fit BeppoSAX spectral model (see Sect. 3.3) applied to the ASCA SIS spectra

Parameter	Observation Date	
	1993	1996
$N_{\text{H}}$ (atom cm $^{-2}$ )	$< 3 \times 10^{19}$	$(5.0 \pm 0.5) \times 10^{20}$
Blackbody kT (keV)	$1.79 \pm 0.02$	$1.66 \pm 0.02$
kT $_e$ (keV)	$7.2 \pm 0.6$	$9.9 \pm 0.9$
$\tau_{\text{p}}$	$23.3 \pm 0.15$	$22.8 \pm 0.3$
kT $_w$ (keV)	$0.153 \pm 0.010$	$0.174 \pm 0.013$
Line energy (keV)	$6.46 \pm 0.03$	$6.49 \pm 0.08$
Line FWHM (keV)	$0.51 \pm 0.08$	$1.65 \pm 0.25$
Line EW (keV)	$0.14 \pm 0.02$	$0.285 \pm 0.040$
Line energy (keV)	$7.06 \pm_{0.04}^{0.02}$	...
Line FWHM (keV)	$< 0.30$	...
Line EW (keV)	$0.065 \pm 0.010$	...
Edge energy (keV)	$1.37 \pm 0.03$	$1.28 \pm 0.03$
Edge $\tau$	$0.093 \pm 0.012$	$0.15 \pm 0.02$
$\chi^2/\text{dof}$	766.0/570	721.5/559

1.5–2.5. The spectrum scattered in an ADC is expected to resemble the original, unless the optical depth is large. The second is the extremely large contribution of the blackbody component ( $\gtrsim 40\%$  of the total), whereas fits to luminous LMXRB indicate the presence of blackbodies with typical luminosities of 16–34% of the non-thermal component (White et al. 1988). However, we note that another LMXRB, the X-ray dip source XB 1746-371 located in the globular cluster NGC 6441, also recently been found to have a strong blackbody-like component which contributes 88% of the 1–10 keV flux (Parmar et al. 1999; see also Guainazzi et al. 2000). The blackbody component most probably originates in an optically thick boundary layer between the accretion disk and the neutron star surface, or from the neutron star itself. It is therefore unlikely to be observed directly in X 1822-371 and so it is surprising that it appears so bright in comparison with the non-thermal component. The third unusual aspect of the spectrum is the presence of the strong low-energy feature, which can be modeled as an absorption edge. The fact that a similar component is also seen in the two ASCA observations implies that this is a stable feature of the spectrum, but not necessarily that it is correctly modeled. However, its nature is highly uncertain. The energy corresponds to K-edges of highly ionized Ne x and neutral Mg, or to an L-edge of moderately ionized Fe. Surprisingly, no strong ( $\tau > 0.05$ ) Fe-K or ( $\tau > 0.18$ ) O-K edges are evident in the spectrum.

Models for the spectrum of X 1822-371 which involve a significant Comptonized component appear plausible. A plasma with kT $_e \sim 5$ –10 keV and a  $\tau_{\text{p}}$  of  $\sim 22$ –26 is required. These values imply a Comptonization parameter  $y = 4kT_e\tau_{\text{p}}^2/m_e c^2$  of  $\sim 25$ –40. Values of  $y > 12$  imply that the emerging spectrum will be saturated and have a

Wien-like shape (e.g., Titarchuk 1994). Guainazzi et al. (2000) show that when the BeppoSAX spectra of a number of LMXRB located in globular clusters are fit with the same continuum model as applied here (a blackbody and COMPTT), then the derived values of  $\tau_p$  and  $kT_e$  are respectively correlated and anti-correlated with the source luminosity. Guainazzi et al. (2000) suggest that these correlations may be qualitatively explained if the X-ray emission at the boundary layer between the accretion disk and the neutron star surface is proportional to the accretion rate. If this results in an increase in the Comptonizing plasma optical depth this would allow Compton cooling to become more efficient, yielding a lower Comptonizing electron temperature. If the intrinsic luminosity of X 1822-371 is assumed to be  $2 \times 10^{37}$  erg s<sup>-1</sup> (see Sect. 1), then the values derived here using BeppoSAX for  $\tau_p$  and  $kT_e$  are in good agreement with the relations derived from the study of the globular cluster LMXRB X-ray sources.

The overall X-ray spectrum of X 1822-371 remains poorly understood. In particular, calculations by e.g., Ko & Kallman (1994) and Kallman et al. (1996) show that photo-ionized ADC should be a rich source of line emission, which does not appear to be the case here as only a moderate EW Fe-K line is seen. Vrtilik et al. (1993) discuss the situation where an X-ray source is viewed at high inclination through a moderate optical depth ADC. They predict both a deep Fe-K edge and a prominent K- $\alpha$  emission line - again neither of which are seen. Thus the X 1822-371 spectrum cannot be easily understood in terms of current models of X-ray production and reprocessing in ADCs and we await future high quality measurements to shed more light on this complex spectrum.

*Acknowledgements.* The BeppoSAX satellite is a joint Italian and Dutch programme. We thank the referee, Martin Still, for helpful comments and Ken Ebisawa, Koji Mukai, and the staff of the BeppoSAX Science Data Center for assistance. This research has made use of data obtained through the High Energy Astrophysics Science Archive Research Center Online Service, provided by the NASA/Goddard Space Flight Center.

## References

- Anders E., Grevesse N., 1989, *Geochimica et Cosmochimica Acta* 53, 197
- Boella G., Chiappetti L., Conti G., et al., 1997, *A&AS* 122, 327
- Frontera F., Costa E., Dal Fiume D., et al., 1997, *A&AS* 122, 371
- Guainazzi M., Parmar A.N., Oosterbroek T., 2000, *Ap. Lett & Comm.* submitted
- Hellier C., Mason K.O., 1989, *MNRAS* 239, 715
- Hellier C., Mason K.O., Williams O.R., 1992, *MNRAS* 258, 457
- Hellier C., Smale A.P., 1994. In: Holt S.S., Day C.S.R. (eds.) *Evolution of X-ray Binaries*, AIP Conf. Ser 308, p. 535
- Hua X.-M., Titarchuk L., 1995, *ApJ* 449, 188
- Kallman T.R., Leidahl D., Osterheld A., Goldstein W., Kahn S., 1996, *ApJ* 465, 994
- Ko Y.-K., Kallman T.R., 1994, *ApJ* 431, 273
- Manzo G., Guarrusso S., Santangelo A., et al., 1997, *A&AS* 122, 341
- Mason K.O., Córdova F.A., 1982, *ApJ* 262, 253
- Mason K.O., Murdin P.G., Tuohy I.R., Seitzer P., Branduardi-Raymont G., 1982, *MNRAS* 200, 793
- Morisson D., McCammon D., 1983, *ApJ* 270, 119
- Parmar A.N., Martin D.D.E., Bavdaz M., et al., 1997, *A&AS* 122, 309
- Parmar A.N., Oosterbroek T., Guainazzi M., et al., 1999, *A&A* 351, 225
- Predehl P., Schmitt J.H.M.M., 1995, *A&A* 293, 889
- Puchnarewicz E.M., Mason K.O., Córdova F.A., 1995, *Adv. Space Res.* 16, 3, 65
- Tanaka Y., Inoue H., Holt S.S., 1994, *PASP* 46, L37
- Titarchuk L., 1994, *ApJ* 434 570
- Titarchuk L., Lyubarskij Y., 1995, *ApJ* 450, 876
- Van Paradijs J., McClintock J.E., 1995. In: Lewin W.H.G., van Paradijs J., van den Heuvel E.P.J. (eds.) *X-ray Binaries*. Cambridge University Press, Cambridge, p. 58
- Vrtilik S.D., Soker N., Raymond J.C., 1993, *ApJ* 404, 696
- White N.E., Holt S.S., 1982, *ApJ* 257, 318
- White N.E., Becker R.H., Boldt E.A., et al., 1981, *ApJ* 247, 994
- White N.E., Stella L., Parmar A.N., 1988, *ApJ* 324, 363
- White N.E., Kallman T.R., Angelini L., 1997. In: Makino F., Mitsuda K. (eds.) *X-Ray Imaging and Spectroscopy of Cosmic Hot Plasmas*, Waseda University, Tokyo, p. 411